Epitaxially strained [001]-$(PbTiO_3)_1(PbZrO_3)_1$ superlattice and $PbTiO_3$ from first principles

Claudia Bungaro* and K. M. Rabe
Department of Physics and Astronomy, Rutgers University, Piscataway, New Jersey 08854-8019, USA
(Received 4 December 2003; published 17 May 2004)

The effect of layer-by-layer heterostructuring and epitaxial strain on lattice instabilities and related ferroelectric properties is investigated from first principles for the [001]-$(PbTiO_3)_1(PbZrO_3)_1$ superlattice and pure $PbTiO_3$ on a cubic substrate. The results for the superlattice show an enhancement of the stability of the monoclinic *r* phase with respect to pure $PbTiO_3$. Analysis of the lattice instabilities of the relaxed centrosymmetric reference structure computed within density functional perturbation theory suggests that this results from the presence of two unstable zone-center modes, one confined in the $PbTiO_3$ layer and one in the $PbZrO_3$ layer, which produce in-plane and normal components of the polarization, respectively. The zero-temperature dielectric response is computed and shown to be enhanced not only near the phase boundaries, but throughout the *r* phase. Analysis of the analogous calculation for pure $PbTiO_3$ is consistent with this interpretation, and suggests useful approaches to engineering the dielectric properties of artificially structured perovskite oxides.

DOI: 10.1103/PhysRevB.69.184101 PACS number(s): 77.84.−s, 77.55.+f, 68.55.−a, 68.35.−p

I. INTRODUCTION

Perovskite oxide superlattices are expected to have properties distinct from those of the bulk constituents. Due to lattice mismatch, constituent layers below the critical thickness generally are in highly strained states. As can be confirmed by first-principles studies of bulk materials, the lattice instabilities and properties of bulk perovskites are extremely sensitive to the strain state. The degree of strain can be further tuned by varying the lattice constant of the substrate on which the superlattice is grown.

This discussion is of practical interest as it has been shown that perovskite oxide superlattices can indeed be grown with atomic scale precision,[1–3] opening up a highly varied family of artificially structured materials for investigation. Thus, first-principles prediction of superlattice properties can directly lead to productive interactions with experimentalists and progress in materials design.[4,5]

In this work, we consider the simplest possible (and as yet hypothetical) [001]-$(PbTiO_3)_m(PbZrO_3)_n$ superlattice with $m=1$ and $n=1$. As shown in Fig. 1, this consists of single unit cell layers of $PbZrO_3$ (PZ) and $PbTiO_3$ (PT) alternating along [001]. The equilibrium cubic lattice constant of bulk PZ is significantly greater than that of PT, with the computed values being $a_{0,PZ}=7.77$ a.u. and $a_{0,PT}=7.37$ a.u., leading to a 5% mismatch (the corresponding experimental values are 7.81 a.u., 7.50 a.u, and 4%). At their equilibrium lattice constants, both cubic PT and cubic PZ have an unstable threefold degenerate polar phonon mode at the zone center. The lattice mismatch means that in the superlattice, PZ is under compressive in-plane stress, while PT is under tensile in-plane stress. If the structure is allowed to relax without breaking the central mirror plane symmetry (i.e., in space group $P4/mmm$), the in-plane lattice constant takes an intermediate value of 7.57 a.u. The PZ unit cell elongates, giving a local tetragonal unit cell with $c/a>1$, and conversely, the PT unit cell will shorten, resulting in a local tetragonal unit cell with $c/a<1$. This lowering of unit cell symmetry leads to a splitting of the threefold degenerate unstable mode in each layer, with the lower frequency mode(s) along the long direction(s). Thus, on qualitative grounds, one expects at least two unstable Γ modes of different symmetry, one associated with polarization along the normal in the PZ layer, and a second, twofold degenerate, mode producing polarization in the plane of the PT layer. Density functional perturbation theory (DFPT) calculations of the phonon dispersion of the relaxed centrosymmetric superlattice show two unstable zone-center polar modes, one with in-plane polarization confined in the PT layer and the other with polarization along the normal confined in the PZ layer, quantitatively confirming this picture.[6] The energy of the system can be lowered by either of these modes alone; the actual ground state might involve choosing one, or the other, or coupling both together.

First principles ground-state-structure calculations have

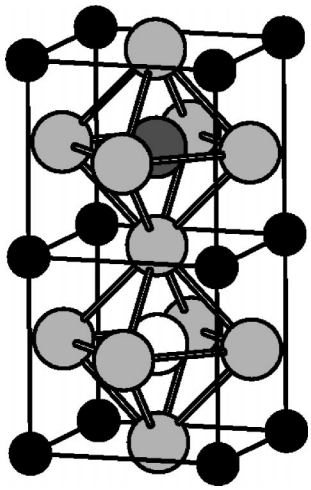

FIG. 1. The ideal double-perovskite ten-atom unit cell of the [001]-$(PbTiO_3)_1(PbZrO_3)_1$ superlattice. The lead, oxygen, titanium and zirconium atoms are indicated by small solid circles, light gray circles, dark gray circles and open circles, respectively. The oxygen octahedra and the ideal perovskite five-atom cells are outlined. The pseudoperovskite c/a is defined as half the unit cell c/a. Note that this is the same structure considered as a ordered realization of PZT in Ref. 7.

previously been performed for this system, regarding the 1:1 [001] ordered PZT 50/50 supercell as an approximate realization of the PZT solid solution.[7] Under the constraint of experimental volume, $c/a=1.035$ and $\alpha=\beta=90°$, it was found that the relaxed structure has monoclinic Cm symmetry, with internal coordinates in reasonable agreement with those experimentally determined for the monoclinic PZT phase.[8] Connecting this result to our discussion in terms of lattice instabilities, we see that the ground state is in fact obtained by freezing in the two modes together, giving a total polarization $\mathbf{P}=(P,P,P_z)$ rotated away from the c axis. Piezoelectric coefficients computed for this structure in Ref. 7 have very large values. This is attributed to the low energy for polarization rotation; this mechanism was first suggested to explain the high piezoelectric response of single crystal PMN-PT (Refs. 9,10) and accounts for the enhancement not only of the piezoelectric response in the monoclinic phase of the superlattice, but also, as we will show below, for the enhancement of the dielectric response.

Under an epitaxial constraint imposed by a cubic [001] substrate, the in-plane lattice vectors are equal in length and make an angle of 90°, while the system is otherwise free to relax. Our qualitative picture of the superlattice instabilities suggests that the two modes should respond differently to changes in the substrate lattice constant. As the substrate lattice constant increases, the mode with polarization along the normal should become higher in frequency, while the mode with in-plane polarization should soften. This change in relative stability is expected to affect the direction of the polarization in the ground-state structure, in a manner consistent with previous calculations in which a different structural constraint, on c/a, was imposed.[7]

In this paper, we present a quantitative first-principles analysis of the effect of varying in-plane strain on the epitaxially constrained $[001]$-$(PbTiO_3)_1(PbZrO_3)_1$ superlattice. In Sec. II, we describe the details of the computations. In Sec. III, we present results of the optimized structural parameters for in-plane lattice constants $a_\parallel$ ranging from well below $a_{0,\mathrm{PT}}$, at which the PT unit cell is expected to be approximately cubic, to above $a_{0,\mathrm{PZ}}$. This wide range of strain allows us more fully to investigate the effects of strain on structure and properties. As we will see, there is a sequence of phases, from the tetragonal c phase at the smallest values of $a_\parallel$, through a monoclinic r phase with increasing a_0 and finally to an orthorhombic aa phase. The locations of the phase boundaries are determined by computing the Hessian matrix of each optimized structure, comprised of the zone-center force-constant matrix, the elastic constants and the quadratic-order coupling between zone-center atomic displacements and homogeneous strain, and extrapolating to zero eigenvalue. Near the phase boundaries and throughout the r phase the dielectric and piezoelectric responses are high, the sensitivity to applied fields and stresses resulting from the ease with which the polarization can be changed through rotation. We relate these results to the lattice instabilities of the centrosymmetric reference structure obtained from DFPT computation of the $\mathbf{q}=0$ frequencies. The behavior of the superlattice is compared with that of pure PT, which is seen to exhibit a qualitatively different behavior. In Sec. IV, we discuss this distinction using a two-mode vs one-mode picture, and suggest some ways that these results can be used in materials design.

II. METHOD

To predict the ground-state structure and zone-center phonon frequencies, we use density functional theory (DFT) and density functional perturbation theory (DFPT) (Refs. 11,12) within the local density approximation (LDA).[13] Calculations in this work have been done using the PWSCF package.[14] We use Vanderbilt ultrasoft pseudopotentials[15] to describe the interaction between ionic cores and valence electrons, and plane-wave basis set with kinetic energy cut-off of 35 Ry. The augmentation charges, required by the use of ultrasoft pseudopotentials, are expanded with an energy cutoff of 350 Ry. Brillouin zone (BZ) integrations are performed with a $6\times6\times3$ Monkhorst-Pack mesh.

The polarization $\mathbf{P}$ is computed using the linearized expression $\mathbf{P}_\alpha=\Sigma_{i\beta}Z^*_{i,\alpha\beta}\,u_{i\beta}$, where $\mathbf{u}_i$ are the atomic displacements of the optimized structure relative to the centrosymmetric reference structure (described below), and Z^* are the atomic Born effective charge tensors. The values of polarization reported below are computed with the averaged effective charge tensors of pure PT and pure PZ given in Table II of Ref. 6, which have been shown to be a good approximation to those of the superlattice.

The epitaxial constraint from a cubic substrate is treated implicitly by constraining the in-plane lattice constant of the system. We consider a range of in-plane strains from -6% to $+4\%$. As the reference in-plane lattice parameter to define the in-plane strain, we use the equilibrium in-plane lattice parameter computed for the optimized polar structure $a_0=7.73$ a.u. for the superlattice and $a_0=7.32$ a.u. for PT. Thus, the system at zero in-plane strain has the minimum elastic energy.

For each value of the in-plane strain, we perform the structural optimization of the superlattice and of pure PT in two stages. First, the ideal double-perovskite 10-atom unit cell of the superlattice is relaxed without any symmetry breaking beyond that associated with the Zr/Ti ordering (tetragonal space group $P4/mmm$, No. 123). Similarly, the perovskite five-atom unit cell of PT is relaxed in space group $P4/mmm$. These will be referred to as the centrosymmetric reference structures. The zone-center phonon modes of these structures are computed using DFPT. This shows the presence or absence of unstable modes that provide a guide to energy-lowering distortions.

Then, the symmetry is broken to allow relaxation into a lower symmetry phase, which we label following the notation of Pertsev *et al.*[16] For the whole range of in-plane strain, we consider relaxations into the c phase (tetragonal space group $P4mm$, No. 99) with polarization $P\hat{z}$, the aa phase (orthorhombic space group $Amm2$, No. 38), with polarization $P(\hat{x}+\hat{y})$, and the r phase (monoclinic space group Cm, No. 8), with polarization $P(\hat{x}+\hat{y})+P_z\hat{z}$. We also investi-

gated the *ac* phase (monoclinic space group Pm, No. 6), with polarization $P\hat{x}+P_z\hat{z}$, and the *a* phase (orthorhombic space group $Pmm2$, No. 25), with polarization $P\hat{x}$; these two phases are found to be energetically unfavorable and do not appear in the present phase diagram. In principle, an equilibrium *c* phase can be obtained by optimizing structural parameters from a starting *r* phase or *ac* phase (and an equilibrium *aa* phase from a starting *r* phase) though in practice more accurate results can be obtained by studying each of the space groups separately. Compatible *k*-point sampling allows us directly to compare the energies of these structures. Although the angle γ between the *c* axis and the plane can in principle vary, in the total energy calculations it is held fixed at 90° to simplify the calculation. The main effect of this approximation is to reduce the range of stability of the *r* phase as a function of in-plane strain; for the systems considered here, we describe below how we compute the effect of strain through analysis of the Hessian matrix.

The zone-center dynamical matrices are computed for the optimized structures using DFPT. The zone-center phonon modes, obtained by diagonalizing the dynamical matrices, are used according to the formalism of Ref. 17 to compute the phonon contribution to the zero-temperature constant-strain static dielectric tensor and to study its dependence upon epitaxial strain. We also used these results for a systematic study of the stability of the various phases as a function of in-plane strain. The full Hessian matrix of the second derivatives of the energy with respect to lattice-periodic atomic displacements and homogeneous strain is constructed with DFPT for the atomic displacements and finite difference stress and force results for the derivatives involving strain. Tracking the lowest eigenvalue of the Hessian matrix, we can accurately identify the instability point of a given phase as the in-plane strain where the lowest eigenvalue becomes negative.[18] This allows a more accurate determination of the position of the phase boundary than total energy calculations alone, which are limited by computational precision, and also allows us to include the effects of the coupling to shear strain η_4 and η_5 in the *r* phase, equivalent to allowing γ to relax from 90°.

III. RESULTS

This section is organized as follows. In Sec. III A, we present the calculations of the equilibrium structural parameters and polarization as a function of in-plane strain. Calculations of zone-center phonon modes, elastic constants, and coupling between the atomic displacements and homogeneous strain are performed to carry out the stability analysis and precisely locate the phase boundaries. In Sec. III B, we present the results of the zone-center phonons in the centrosymmetric reference structure as a function of in-plane strain and use them to interpret the phase diagram. In Sec. III C, we present the in-plane-strain dependence of the static dielectric tensor. Results in each subsection are presented first for the superlattice and then, for comparison, for pure PT.

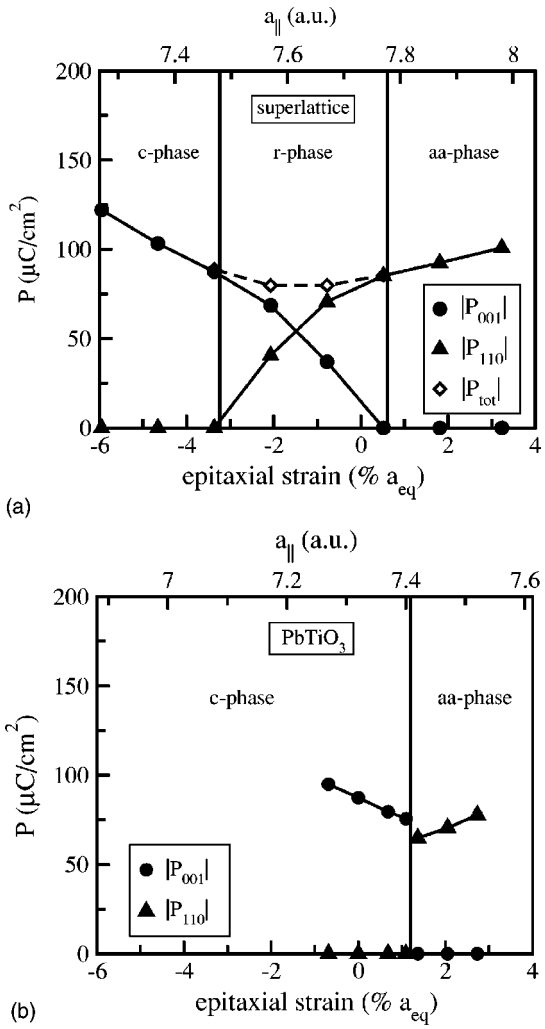

FIG. 2. Components of the polarization along the [001] and [110] directions, and its magnitude $|\mathbf{P}_{tot}|$, as a function of in-plane strain for (a) the $[001]$-$(PbTiO_3)_1(PbZrO_3)_1$ superlattice and (b) pure PT.

A. Structural parameters and phase diagram

In Fig. 2(a) we show the structural phase transitions of the superlattice with varying in-plane strain. The symmetry is evident from the nonzero components of the polarization. There is a continuous (second-order) transition from the *c* phase, stable at large compressive in-plane strain, to the *r* phase. In the *r* phase, the polarization has almost constant magnitude and rotates smoothly in the $(1\bar{1}0)$ plane from $\hat{z}$ to $\hat{x}+\hat{y}$, followed by a second continuous transition from the *r* phase to the *aa* phase, stable at large tensile in-plane strain. The in-plane-strain dependence of the energy in each of these three symmetries is shown in Fig. 3(a). The *a*- and *ac*-phase energies computed at $a_{\parallel}=7.57$ a.u. were found to be significantly higher than that of the *r* phase and thus are not included in further discussion. Accurate positions of the second-order *c*-*r* and *r*-*aa* phase boundaries can be best obtained not from intersection points of the total energy curves, but by interpolating the dependence of

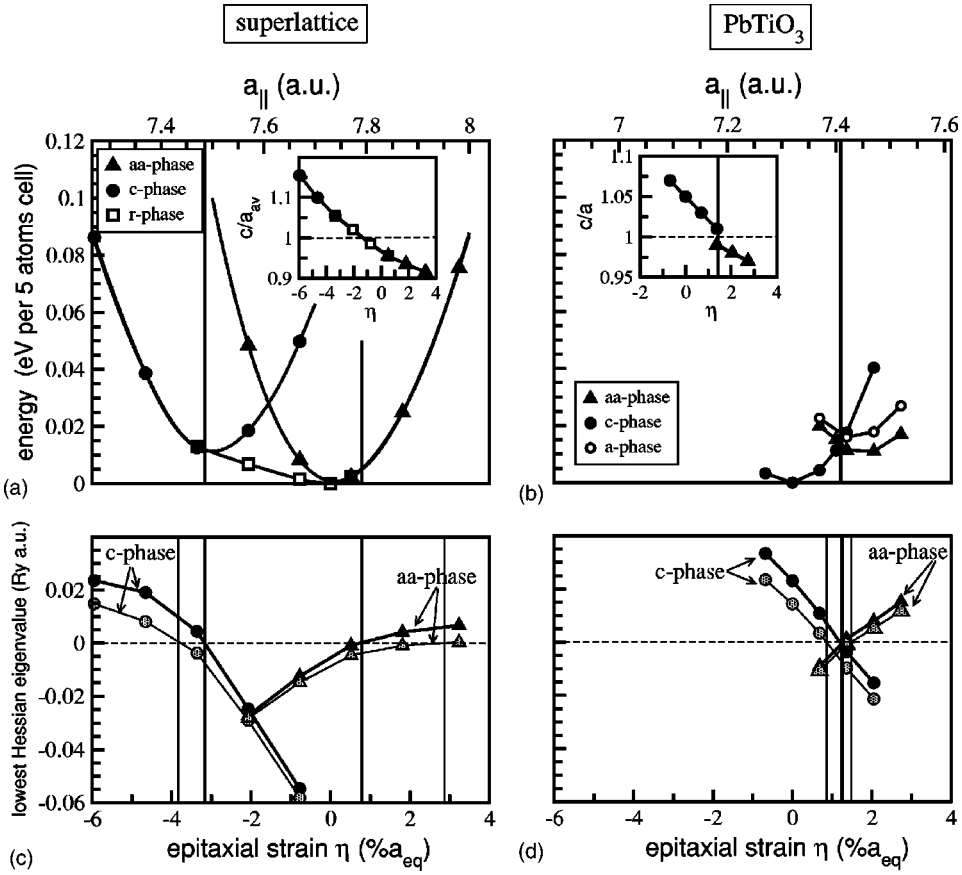

FIG. 3. The energy as a function of in-plane strain for the *c*, *aa*, and *r* phases, for (a) the $[001]$-$(PbTiO_3)_1(PbZrO_3)_1$ superlattice and (b) pure PT. The same scales are used for both systems to facilitate comparison. The insets show the tetragonality c/a as a function of in-plane strain. The lowest eigenvalue of the Hessian, for (c) the $[001]$-$(PbTiO_3)_1(PbZrO_3)_1$ superlattice and (d) pure PT. The circles are for the *c* phase and the triangles for the *aa* phase. The solid symbols are the eigenvalues when only tetragonal strain is allowed, corresponding to the first-principles results in (a) and (b). The open symbols show the change when coupling to shear strain is included, resulting in an enhancement of the stability of the *r* phase.

the quadratic-order energy around the equilibrium phase at each in-plane strain to obtain the in-plane strain at which the instability occurs.

We compute the Hessian matrix (phonons plus tetragonal strain, the latter coupling being zero for the *c* and *aa* phases) and plot the lowest eigenvalue in Fig. 3(c). The zero crossing of the eigenvalues can be seen to correspond to the points where the *r* phase becomes more stable in Fig. 3(a); in the case of the *r*-*aa* transition the critical in-plane strain is clearly much easier to determine accurately in Fig. 3(c). To test the effect of fixing γ to 90°, we also compute the full Hessian matrix, including coupling to shear strains η_4 and η_5, and plot the lowest eigenvalue in Fig. 3(c). It can be seen that the effect of the additional strain relaxation is to expand the region of stability of the *r* phase, the effect being slight for the *c*-*r* boundary and more significant for the *r*-*aa* boundary.

The corresponding results for pure $PbTiO_3$ present an informative contrast to those for the superlattice. In Fig. 2(b) we show the structural phase transitions of pure PT with varying in-plane strain. The system makes a weakly first-order direct transition from the *c* phase at large compressive in-plane strain to the *aa* phase at large tensile in-plane strain. The intermediate *r* phase present in the superlattice has been eliminated. There are small discontinuities in the c/a ratio [inset of Fig. 3(b)] and the magnitude of the polarization at the phase transition. The optimized energies for each symmetry as a function of in-plane strain are shown in Fig. 3(b). Optimization in the monoclinic space group corresponding to the *r* phase produces either the *c*- or *aa* phase depending on in-plane strain; these energies lie very slightly higher than those obtained by optimizing in the tetragonal space groups, reflecting the convergence criterion for the relaxation. We can confirm the weakly discontinuous nature of this transition by computing the Hessian matrix (phonons plus tetragonal strain) and plotting the eigenvalues in Fig. 3(d). At the transition in-plane strain, each of the two phases is marginally stable. To test the effect of fixing γ to 90°, we also compute the full Hessian matrix, including coupling to shear strains η_4 and η_5, and plot the lowest eigenvalue in Fig. 3(d). It can be seen that the effect of the additional strain relaxation introduces a narrow region of stability of the *r* phase, between in-plane strains of 0.86 and 1.48 %. This window of 0.62% is about three times smaller than the $T=0$ width of 2% obtained by Pertsev *et al.*,[16] the latter being an extrapolation to low temperature of a Landau theory fit near the paraelectric-ferroelectric transition temperatures above 700 K.

B. Lattice instabilities of the centrosymmetric reference structure

Next, we investigate the relation of the ground-state structure to the zone-center phonon modes in the centrosymmetric reference structure. In the unstrained superlattice ($a_\parallel = 7.57$ a.u.), there are two unstable, nearly degenerate, polar zone-center modes, an E_u mode with displacements confined in the PT layer and an A_{2u} mode confined in the PZ layer.[6,19] In Fig. 4 we see that these behave differently with increasing in-plane strain, the PZ-like mode being stabilized by increas-

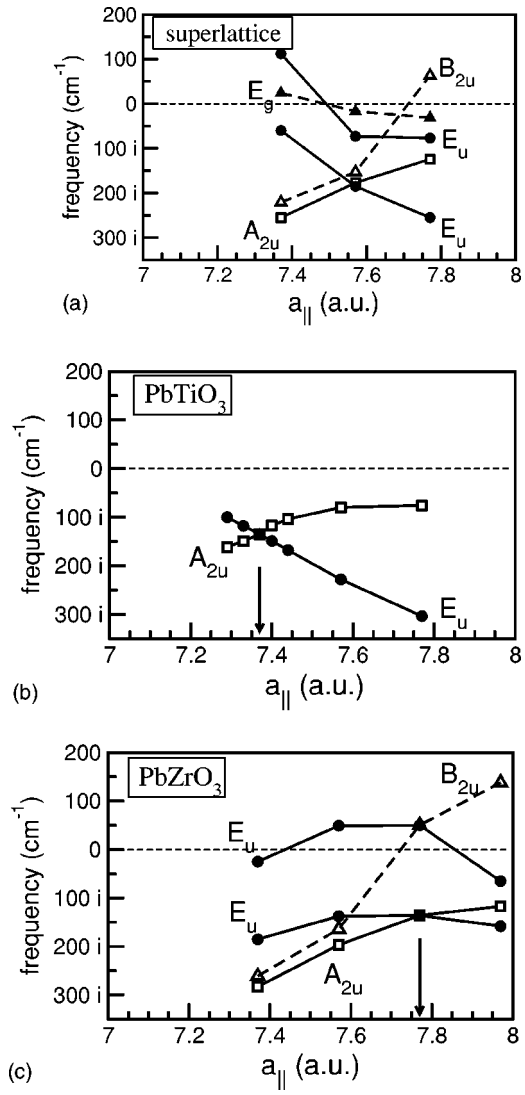

FIG. 4. Frequencies of the unstable zone-center phonons of the centrosymmetric reference structure as a function of in-plane lattice constant for (a) the $[001]$-$(PbTiO_3)_1(PbZrO_3)_1$ superlattice, (b) pure PT, and (c) pure PZ. All modes are labeled by their symmetry; solid (open) symbols indicate modes with displacements perpendicular (parallel) to the *c* axis. Solid and dashed lines connect the plotted points as a guide to the eye, indicating polar and nonpolar character of the modes, respectively. Vertical arrows indicate the lattice parameter of cubic PT and PZ.

ing in-plane strain, while the PT-like mode becomes increasingly unstable. This is consistent with the qualitative picture discussed in the Introduction, with the mode with polarization along the normal being raised in frequency by increasing in-plane lattice constant, while the in-plane mode softens. The ground state structure reflects these opposing trends in the strength of the two unstable modes. At the smallest in-plane lattice constant, it is energetically favorable to freeze in only the A_{2u} mode, producing the *c* phase. As the in-plane lattice constant increases, the in-plane E_u mode softens to the point that it also contributes to the ground state, producing the *r* phase. The frequencies of the two modes cross at an in-plane lattice constant roughly in the middle of the *r* phase. With further increase of the in-plane lattice constant, the A_{2u} mode stiffens to the point that the E_u mode is the only mode contributing to the ground state, producing the *aa* phase. The analysis of the Hessian matrix in the ground state structures shows that the freezing-in of the polar modes eliminates the nonpolar instabilities also seen in Fig. 4, most notably the B_{2u} mode.

The behavior of pure PT is qualitatively similar. There are two unstable polar zone-center modes A_{2u} and E_u, increasing and decreasing in frequency with increasing lattice constant, respectively. The crossing of the two modes is likewise very close to the *c*-*aa* phase boundary, where the *r* phase appears when shear strain relaxation is allowed.

For comparison with the unstable modes in the superlattice, in Fig. 4(c) we show the in-plane strain dependence of the zone-center unstable modes of pure PZ. For the unstrained superlattice we have previously shown[6] that the atomic displacements of the lowest E_u mode, mainly confined in the PT layer, are very close to the displacements of the polar unstable mode of PT bulk. Similarly the atomic displacements of the lowest A_{2u} mode, mainly confined in the PZ layer, are very close to the displacements of the polar unstable mode of PZ bulk. By comparing the phonon frequencies in Fig. 4, we see that certain modes in the superlattice can be identified with modes in pure strained PT and PZ. The PT-like mode of the superlattice, the lowest E_u mode, has a strain-dependent frequency very similar to that of the lowest E_u mode of pure PT. The PZ-like mode of the superlattice, A_{2u} mode, compares well with the A_{2u} mode of pure PZ. The B_{2u} mode in the superlattice is a PZ-like mode with O displacements mainly confined in the PZ layer and its strain-dependent frequency closely corresponds to that of the B_{2u} mode of pure PZ.

C. Static dielectric tensor

The phonon contribution to the static dielectric tensor computed as a function of epitaxial strain is presented for the superlattice in Figs. 5(a) and 5(c). In (a), we plot the component ϵ_{zz}, as for thin films this is relevant to the dielectric screening of an electric field applied across the film. It can be seen that this component diverges on both sides of the *r*-*aa* phase boundary, and is large in a substantial fraction of the *r* phase. In all three phases of interest, the polarization lies in the $(1\bar{1}0)$ plane. To simplify the form of the dielectric tensor, we have chosen the *x*, *y*, and *z* axes to be parallel to the $[110]$, $[1\bar{1}0]$, and $[001]$ directions in the (doubled) cubic perovskite cell, respectively [in the discussion below, we continue to specify directions and planes with respect to the original (doubled) cubic perovskite cell axes]. In this basis the dielectric tensor for the *c* and *aa* phases are diagonal, while the dielectric tensor for the *r* phase has a nonzero *xz* component. Diagonalizing the dielectric tensor for the *r* phase allows us to plot the inverses of the three eigenvalues ϵ_1, ϵ_2, and ϵ_3 in Fig. 5(c); note that a value approaching zero in the plot corresponds to a divergence of ϵ. In the *c* and *aa* phases, all three eigenvectors are uniquely determined by symmetry. In the *c* phase $\epsilon_3 = \epsilon_{zz}$ is the ''collinear'' response, i.e., for a field applied along the direction of the spontaneous

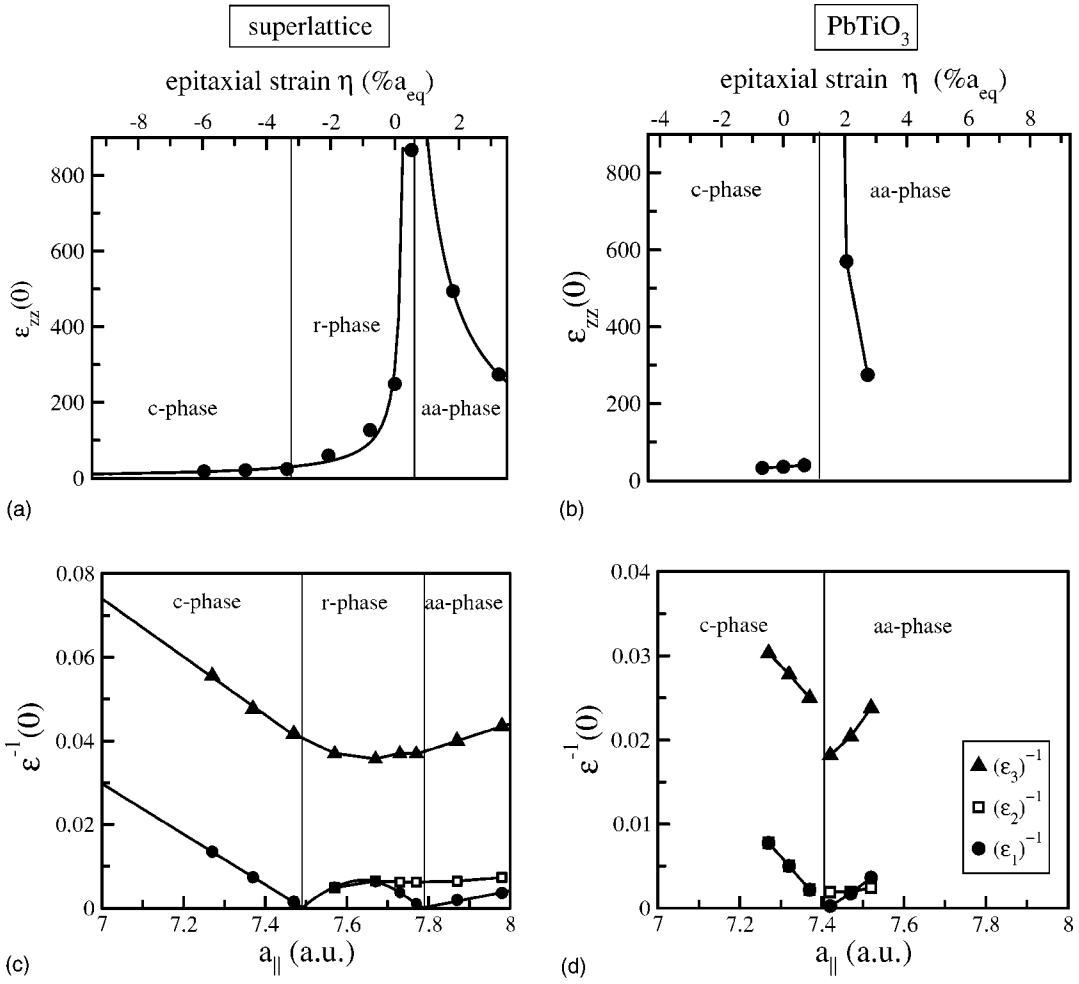

FIG. 5. The phonon contribution to the static dielectric tensor component ϵ_{zz} as a function of the in-plane lattice constant for (a) the $[001]$-$(PbTiO_3)_1(PbZrO_3)_1$ superlattice and (b) pure PT. Inverses of the eigenvalues of the phonon contribution to the dielectric tensor ϵ_1, ϵ_2, and ϵ_3 as a function of the in-plane lattice constant for (c) the $[001]$-$(PbTiO_3)_1(PbZrO_3)_1$ superlattice, and (d) pure PT. The directions of the corresponding eigenvectors are specificed in Sec. III C. The lines are a guide to the eye.

polarization, and $\epsilon_1=\epsilon_2=\epsilon_{xx}=\epsilon_{yy}$. In the *aa* phase, $\epsilon_3=\epsilon_{xx}$ is the collinear component, along $[110]$, $\epsilon_2=\epsilon_{yy}$ is the in-plane component perpendicular to the polarization, and $\epsilon_1=\epsilon_{zz}$ is along the direction normal to the layers. In the *r* phase, the lower symmetry implies that the directions of the eigenvectors are not fully determined by symmetry alone. The ϵ_3 eigenvector is approximately, but not exactly, along the polarization direction, in the $(1\bar{1}0)$ plane. The ϵ_1 eigenvector is perpendicular to the ϵ_3 eigenvector, in the $(1\bar{1}0)$ plane, and the $\epsilon_2=\epsilon_{yy}$ eigenvector is along the in-plane direction $[1\bar{1}0]$. Two eigenvalues of the dielectric tensor ($\epsilon_1=\epsilon_2$) diverge at the continuous *c*-*r* transition, and one (ϵ_1) at the continuous *r*-*aa* transition, through there the second noncollinear eigenvalue ϵ_2 is also fairly large.

In PT [Figs. 5(b) and 5(d)], the behavior of the dielectric constant in the *c* and *aa* phases is rather similar to that in the superlattice, with a near divergence in ϵ_{zz} as the boundary of the *aa* phase is approached. However, comparison of Figs. 5(a) and 5(b) show that the enhancement of the *r* phase in the superlattice gives a large ϵ_{zz} over a much larger range of epitaxial strain.

IV. DISCUSSION

The most striking features of the phase diagram of the epitaxially constrained $[001]$-$(PbTiO_3)_1(PbZrO_3)_1$ superlattice are the width of the *r* phase, the separation of the minimum energy in-plane lattice constants of the *c* and *aa* phases, and the linearity of the energy with in-plane strain in the *r* phase. These have significant implications for the coherence of lattice-mismatched thin films and for the dielectric response.

From Fig. 3(a), it can be seen that the elastic energy of the superlattice as a function of in-plane lattice constant is not parabolic. Rather, as the in-plane lattice constant decreases from 7.73 a.u., the energy rises linearly with a small slope to the minimum of the *c* phase at 7.50 a.u., behaving parabolically only for smaller $a_\parallel$. This makes the film compliant to a broad range of substrates; the estimated critical thickness of fully coherent films is close to constant in this range. For tetragonal $PbTiO_3$, in comparison, within each phase (*c* or *aa*), the energy function is parabolic, so the critical thickness behaves as usual, increasing inversely to the deviation of the in-plane lattice constant from the equilibrium value for that phase.

Based on the computed energies for the various phases of the superlattice in Fig. 3(a), one can predict the occurrence of structural phase transitions with increasing thickness, as the system changes from fully coherent to partially relaxed and finally to fully relaxed. For systems under compressive stress from the substrate, there should be a transition from the *c* phase to the *r* phase with increasing thickness, while for systems under tensile stress, a transition from the *aa* phase to the *r* phase is expected. For pure PT, systems under tensile stress are predicted to undergo a transition with increasing thickness from the *aa* phase through a narrow *r* phase into the *c* phase.

The present analysis identifies the most stable superlattice structure with the ten-atom cell shown in Fig. 1. The possibility remains that there may be instabilities to structural distortions that double or further expand the unit cell, in the plane, along the stacking direction, or both. This may be relevant for making comparisons with experimental observations.

Certain components of the dielectric tensor diverge as the phase boundaries are approached. While the polarization induced by an electric field along the direction of the spontaneous polarization is rather modest, the noncollinear responses are of great interest. This polarization rotation mechanism, through the coupling of polarization and strain, has been invoked to explain the large piezoelectric response in single-crystal relaxors,[9,10] and to explain the large piezoelectric response computed for ordered PZT (with the same structure as the superlattice considered here) in Ref. 7. The *r* phase, with its continuously variable direction for the spontaneous polarization, is expected to have particularly large responses. In particular, the zz component of ϵ, the normal polarization induced by a field along the normal, will be enhanced by a noncollinear contribution throughout the *r* phase.

Finally, we consider the origin of the different behavior of the two systems. First, we discuss the difference in equilibrium lattice constant of the *c* phase and the *aa* phase. In a simple perovskite, such as pure PT, the difference arises from coupling between the strain and the unstable polar mode. PT has an unusually strong strain coupling, leading to a c/a of about 1.06 in the tetragonal ground state; the *c*-phase and *aa*-phase equilibrium in-plane lattice constants are 7.32 and 7.45 a.u., respectively. Analogous information about the behavior of pure PZ can be obtained from the published parametrization of first-principles results[20] with the *c*-phase and *aa*-phase equilibrium in-plane lattice constants being 7.71 and 7.83 a.u., respectively. A simple elastic-energy model for the superlattice can be constructed as the sum of the elastic energies of the two layers. For each constituent, the elastic constants of the *c* and *aa* phases turn out to be similar, with the values for PZ about 70% larger than those for PT. In the superlattice, the first-principles equilibrium in-plane lattice constant of the *c* phase is 0.07 a.u. less than that of the elastic-energy model, and in the *aa* phase it is 0.05 a.u. greater, leading to a separation of the first-principles lattice constants of the two phases about twice as large as in the model. This deviation from a simple elastic energy model might be due to the thinness of the individual layers and/or to the importance of interlayer interactions beyond lattice matching.

The stability of the *r* phase is favored by in-plane and perpendicular unstable polar modes having both a similar strength and positive anharmonic coupling. In a simple perovskite, such as pure PT, tetragonal strain splits the threefold degenerate mode to give a dominant unstable A_{2u} mode for c/a less than 1, and a dominant in-plane E_u mode for c/a greater than 1. If the ground state is obtained by freezing in only the dominant unstable mode, we expect a discontinuous change in character at the in-plane lattice constant corresponding to the lowest-energy cubic structure, as seen in PT. Even if the strengths of the two modes are similar, the fourth order anharmonic term coupling them must be large enough to favor this combination over the higher-symmetry structures (z, as in the *c* phase, or along [110] as in the *aa* phase). Its magnitude can vary greatly from material to material, being enhanced by coupling to particular types of strain, especially shear strain.

In the superlattice, it seems that separating the two components of the polarization in two spatially distinct regions helps to stabilize the *r*-phase structure. Even if the strengths of the unstable polar modes in the two layers are different, a low-energy structure can be obtained by combining the perpendicular mode with polarization along z in one layer (e.g., the PZ layer) with a mode of different character, with polarization along [110], in the other layer (e.g., the PT layer). This idealized picture will be somewhat modified by electrostatic considerations, which will tend to minimize the divergence of **P** by polarizing the PT layer along the z direction. The usefulness of this simple picture lies in its applicability to longer period PT/PZ superlattices; such systems are also of interest as they are accessible to experimental investigation.

V. CONCLUSIONS

The phase diagrams for the $[001]$-$(PbTiO_3)_1(PbZrO_3)_1$ superlattice and pure PT with varying in-plane strain on a cubic substrate have been obtained from first-principles density-functional total-energy calculations and a stability analysis involving the computation of zone-center phonons and their coupling to strain. At the smallest $a_\parallel$, both systems are tetragonal with pseudoperovskite c/a greater than 1 and **P** along [001] (the *c* phase), and at the highest $a_\parallel$, both are pseudotetragonal orthorhombic with pseudoperovskite c/a less than 1 and **P** along [110] (the *aa* phase). However, at intermediate in-plane strain, the transitional behavior is quite different. In the superlattice, **P** rotates away from the normal to give a monoclinic structure (the *r* phase), and at a higher value of $a_\parallel$, completes the rotation into the plane of the layers. In the monoclinic phase, the dielectric and piezoelectric response is high, the sensitivity to applied fields and stresses resulting from the ease with which the polarization can be changed through rotation. In contrast, in pure PT changing epitaxial strain results in a discontinuous transition from **P** along [001] to **P** in plane if only tetragonal strain is allowed, with full coupling to shear strain opening a narrow range of *r*-phase stability. While the characteristic divergence

of certain components of the dielectric tensor is seen as the phase boundaries are approached, there is no significant contribution from polarization rotation. For both systems, we relate the observed ground states to the instabilities of a relaxed centrosymmetric structure computed via DFPT. From these results we conclude that in the superlattice, the presence of two unstable modes confined in different layers, of different symmetry and comparable strength significantly enhances the window for the monoclinic structure, which suggests new approaches for designing artificially structured materials with high dielectric and piezoelectric response.

ACKNOWLEDGMENTS

We thank D. Vanderbilt, J. Neaton, O. Dieguez, A. Antons, S. Tinte, M. H. Cohen, and H. Krakauer for valuable discussions. This work was supported by Grant No. ONR N00014-00-1-0261. The work of K.M.R. was performed in part at LMCP, Université de Paris VI and Materials Department, University of California at Santa Barbara. The majority of the computations were performed at the Department of Defense High Performance Computing Centers NAVO and ERDC.

*Electronic address: bungaro@physics.rutgers.edu

[1] J.C. Jiang, X.Q. Pan, W. Tian, C.D. Theis, and D.G. Schlom, Appl. Phys. Lett. **74**, 2851 (1999).
[2] M.P. Warusawithana, E.V. Colla, J.N. Eckstein, and M.B. Weissman, Phys. Rev. Lett. **90**, 036802 (2003).
[3] J. Sigman, D.P. Norton, H.M. Christen, P.H. Fleming, and L.A. Boatner, Phys. Rev. Lett. **88**, 097601 (2002).
[4] J.B. Neaton, C.L. Hsueh, and K.M. Rabe, in *Perovskite Materials*, edited by K. Poeppelmeier, A. Navrotsky, and R. Wentzcovitch, Mater. Res. Soc. Symp. Proc. No. 718 (Materials Research Society, Warrendale, 2002).
[5] J.B. Neaton and K.M. Rabe, Appl. Phys. Lett. **82**, 1586 (2003).
[6] C. Bungaro and K.M. Rabe, Phys. Rev. B **65**, 224106 (2002).
[7] Z. Wu and H. Krakauer, Phys. Rev. B **68**, 014112 (2003).
[8] B. Noheda, D.E. Cox, and G. Shirane, Appl. Phys. Lett. **74**, 2059 (1999).
[9] H.X. Fu and R.E. Cohen, Nature (London) **403**, 281 (2000).
[10] S.E. Park and T.R. Shrout, J. Appl. Phys. **82**, 1804 (1997).
[11] P. Hohenberg and W. Kohn, Phys. Rev. **136**, B864 (1964); W. Kohn and L.J. Sham, Phys. Rev. **140**, A1133 (1965).
[12] S. Baroni, S. de Gironcoli, A. Dal Corso, and P. Giannozzi, Rev. Mod. Phys. **73**, 515 (2001).
[13] D.M. Ceperley and B.J. Alder, Phys. Rev. Lett. **45**, 566 (1980); J.P. Perdew and A. Zunger, Phys. Rev. B **23**, 5048 (1981).
[14] S. Baroni, A. Dal Corso, S. de Gironcoli, and P. Giannozzi, http://www.pwscf.org
[15] D. Vanderbilt, Phys. Rev. B **41**, 7892 (1990).
[16] N.A. Pertsev, A.G. Zembilgotov, and A.K. Tagantsev, Phys. Rev. Lett. **80**, 1988 (1998).
[17] G.-M. Rignanese, X. Gonze, and A. Pasquarello, Phys. Rev. B **63**, 104305 (2001); G.-M. Rignanese, F. Detraux, X. Gonze, and A. Pasquarello, *ibid.* **64**, 134301 (2001).
[18] A. Garcia and D. Vanderbilt, Phys. Rev. B **54**, 3817 (1996).
[19] We have classified the phonon modes according to the irreducible representations of $P4/mmm$, using the Mulliken symbols E_u, A_{2u}, B_{2u}, and E_g that correspond to the modes Γ_5', Γ_1', Γ_3', and Γ_5, respectively, in the nomenclature we used in Ref. 6.
[20] R.D. King-Smith and D. Vanderbilt, Phys. Rev. B **49**, 5828 (1994).